# A high resolution free surface model of the Mediterranean Sea

M. Tonani, N. Pinardi, S. Dobricic, I. Pujol, C. Fratianni

Ocean Sci. Discuss., 4, 213–244, 2007
www.ocean-sci-discuss.net/4/213/2007/


Ocean Science Discussions

Papers published in *Ocean Science Discussions* are under open-access review for the journal *Ocean Science*

# A high resolution free surface model of the Mediterranean Sea

**M. Tonani[1], N. Pinardi[2], S. Dobricic[1], I. Pujol[1], and C. Fratianni[1]**

[1]Istituto Nazionale di Geofisica e Vulcanologia, Bologna, Italy
[2]University of Bologna, Corso di Scienze Ambientali, Ravenna, Italy

Received: 8 January 2007 – Accepted: 4 February 2007 – Published: 26 February 2007

Correspondence to: M. Tonani (tonani@bo.ingv.it)

## Abstract

This study describes a new model implementation for the Mediterranean Sea which has the presently highest vertical resolution over the Mediterranean basin. The resolution is of 1/16°×1/16° in horizontal and 71 unevenly spaced vertical levels. This model has been developed in the frame of the EU-MFSTEP project and it is the operational forecast model presently used at the basin scale.

For the first time in the Mediterranean, the model considers an implicit free surface and this characteristics enhances the model capability to simulate the sea surface height variability.

In this study we show the calibration/validation experiments done before and after the model has been used for forecasting. The first experiment consist of six years of a simulation forced by a perpetual year forcing and the other experiment is a simulation from January 1997 to December 2004, forcing the model with 6 h atmospheric forcing fields from ECMWF. For the first time the model Sea Level Anomaly is compared with SLA and with ARGO data to provide evidence of the quality of the simulation.

The results show that this model is capable to reproduce most of the variability of the general circulation in the Mediterranean Sea even if some basic model inadequacies stand out and should be corrected in the near future.

## 1 Introduction

The aim of this study is to give a detailed description of the Mediterranean Sea forecasting model implementation studies done during the MFSTEP project in order to assess the quality of the numerical model which is now used for the daily forecasts at the basin scale.

The first model used for forecasting at the basin scale has been described by Pinardi et al., (2003). The previous implementation consisted of a version of the Modular Ocean Model (MOM) with 1/8×1/8 degrees horizontal resolution and 31 levels in verti-



OSD

4, 213–244, 2007

cal. The present model is a version of the Ocean PArallelilsè-OPA code (Madec et al., 1998) and its horizontal and vertical resolution is the highest presently available for the Mediterranean Sea: 1/16°×1/16° degrees in horizontal (approx. 6.5 km) and 71 vertical levels. The level of depths are unevenly spaced and have a thickness ranging from 3m at the surface to 300 m at the ocean bottom. The depth of the first level is 1.5 m and of the deepest is 5000 m. The model could be therefore defined as a mesoscales resolving model for the Mediterranean Sea since the first internal Rossby radius of deformation is around 10–15 km in summer and for most of the Mediterranean subregional Seas (with the exception of the Adriatic Sea). The model is also new for the Mediterranean Sea since it uses an implicit free surface parameterisation instead of a rigid lid as for all the other models implemented for the region (Demirov and Pinardi, 2002; Beranger et al., 2004).This allows to have a water flux forcing for the model in equilibrium with the salt flux.

This paper is organized in the following way: Sect. 2 gives a detailed description of the model equations and parameter choices, Sect. 3 describes the experimental design, Sect. 4 describes the simulation results and the comparison with the observations and Sect. 5 offers the conclusions.

## 2 Model equations and parameter choices

### 2.1 Model equations and domain of implementation

The model uses the primitive equations with the Boussinesq and incompressible approximations written in spherical coordinates $(\lambda, \varphi, z)$, where $\varphi$ is the latitude, $\lambda$ the longitude and $z$ the depth. The set analytical expressions for the equations are:

$$\frac{\partial u}{\partial t} = (\zeta + f)\, v - w\frac{\partial u}{\partial z} - \frac{1}{2a\cos\varphi}\frac{\partial}{\partial \lambda}\left(u^2 + v^2\right) - \frac{1}{\rho_0 a\cos\varphi}\frac{\partial p}{\partial \lambda} - A^{lm}\nabla^4 u + \frac{\partial}{\partial z}\left(A^{vm}\frac{\partial u}{\partial z}\right) \quad (1)$$



OSD
4, 213–244, 2007

$$\frac{\partial v}{\partial t} = -(\zeta + f)\, u - w\frac{\partial v}{\partial z} - \frac{1}{2a}\frac{\partial}{\partial \varphi}\left(u^2 + v^2\right) - \frac{1}{\rho_0 a}\frac{\partial p}{\partial \varphi} - A^{lm}\nabla^4 v + \frac{\partial}{\partial z}\left(A^{vm}\frac{\partial v}{\partial z}\right) \quad (2)$$

$$\frac{\partial \theta}{\partial t} = -\frac{1}{a\cos\varphi}\left[\frac{\partial}{\partial \lambda}(\theta u) + \frac{\partial}{\partial \varphi}(\cos\varphi \theta v)\right] - \frac{\partial}{\partial z}(\theta w) - A^{lT}\nabla^4 T + A^{vT}\frac{\partial^2 \theta}{\partial z^2} + \delta\mu\,(\theta^* - \theta) \quad (3)$$

$$\frac{1}{a\cos\varphi}\left(\frac{\partial u}{\partial \lambda} + \frac{\partial}{\partial \varphi}[\cos\varphi v]\right) + \frac{\partial w}{\partial z} = 0 \quad (4)$$

$$\frac{\partial \theta}{\partial t} = -\frac{1}{a\cos\varphi}\left[\frac{\partial}{\partial \lambda}(\theta u) + \frac{\partial}{\partial \varphi}(cos\varphi \theta v)\right] - \frac{\partial}{\partial z}(\theta w) - A^{lT}\nabla^4 T + A^{vT}\frac{\partial^2 \theta}{\partial z^2} + \delta\mu(\theta^* - \theta) \quad (5)$$

$$\frac{\partial S}{\partial t} = -\frac{1}{a\cos\varphi}\left[\frac{\partial}{\partial \lambda}(Su) + \frac{\partial}{\partial \varphi}(cos\varphi Sv)\right] - \frac{\partial}{\partial z}(Sw) - A^{lS}\nabla^4 T + A^{S}\frac{\partial^2 S}{\partial z^2} + \delta\mu(S^* - S) \quad (6)$$

$$\rho = \rho(T, S, p) \quad (7)$$

where we recognize that the momentum equations have been re-written in their vorticity form (Pedlosky, 1983). In (1) through (7) $u, v, w$ are the components of the velocity vector, $\varsigma = \frac{1}{a\cos\varphi}\left(\frac{\partial v}{\partial \lambda} - \frac{\partial}{\partial \varphi}[u\cos\varphi]\right)$ is the vorticity, $a$ the earth radius, $f = 2\Omega\sin\varphi$ the Coriolis term with $\Omega$ the constant earth rotation rate, $p$ the hydrostatic pressure, $\theta$ the potential temperature, $S$ the salinity, $\rho$ the in situ density and $\rho_o = 1020\ kg/m^3$ the reference density, $A^{lm}$, $A^{vm}$ the horizontal and vertical eddy viscosities, $A^{vT}$, $A^{vS}$ the vertical diffusivities, $A^{lT}$, $A^{lS}$ the horizontal diffusivities, $\delta$ and $\mu$ are the relaxation coefficients which will be described in details later.

The numerical model code that discretises Eq. (1) through (7) is OPA (Ocean PArallelise) version 8.1 described in Madec et al. (1998). Here we use the OPA version with the implicit free surface so that the latter, denoted by $\eta$, is a prognostic variable. The numerical scheme for the free surface is described by Roullet et al., (2000).

The model domain and the bathymetry are shown in Fig. 1, there are 49 islands and this implementation is named MFS1671. The procedure used to make the coastline,

the bathymetry and the vertical level distribution is described in the Appendix. The Atlantic box is very large with respect to previous implementations (Demirov and Pinardi, 2002) and it will be described in details below.

### 2.2 Sub grid scale parameterizations

The horizontal eddy viscosity ($A^{lm}$) is considered to be a constant value of $5.10^9\ m^4/s$ while the horizontal diffusivities ($A^{lT}, A^{lS}$) are equal and set to the value of $3.10^9\ m^4/s$. The vertical diffusivities ($A^{vS}, A^{vT}$) and viscosity ($A^{vm}$) are a function of the Richardson number as parametrized by Pakanowsky and Philander-PP (1981), i.e.:

$$A^{vt} = \frac{100\times10^{-4}}{(1 + 5(N^2/(\partial U_h/\partial z)^2))^2} + (1.5\times10^{-4}) \tag{8}$$

$$A^{vm} = \frac{A^{vT}}{(1 + 5(N^2/(\partial U_h/\partial z)^2)} + (3\times10^{-4}) \tag{9}$$

where the vertical salinity diffusivity is equal to (8). The PP parameterization is thought to be relevant for mixed layer processes while deep convection needs another parametrization. Thus the model uses enhanced vertical diffusion to produce deep convection: the vertical diffusivity and viscosity coefficients are assigned to be equal 1 $m^2/s$ in regions where the stratification is unstable.

### 2.3 Vertical boundary conditions

At the bottom, $z = -H(x, y)$, we impose:

a) for the vertical velocity:

$$w = -\boldsymbol{u}_h^b \times \nabla H \tag{10}$$

where $\boldsymbol{u}_h^b = (u_b, v_b)$ is the bottom velocity assumed to be the deepest layer velocity;



OSD
4, 213–244, 2007





EGU

b) for the momentum, temperature and salt flux:

$$A^v m \frac{\partial}{\partial z}(\boldsymbol{u}_h)\Big|_{z=-H} = C_D\sqrt{u_b^2 + v_b^2} + e_b \boldsymbol{u}_h^b \tag{11}$$

$$A^v T, S \frac{\partial}{\partial z}(T, S)\Big|_{z=-H} = 0 \tag{12}$$

where $C_D$=$10^{-3}$ is the drag coefficient and $e_b$ is the bottom eddy kinetic energy due to the tides, internal waves breaking and to all the other contributions at very short spatial and temporal scales.

At the surface, $z = \eta$, the boundary conditions are: a) for the vertical velocity

$$\frac{D\eta}{Dt} - (E - P) \tag{13}$$

where $\frac{D\eta}{Dt} = \frac{\partial \eta}{\partial t} + \boldsymbol{u}_h \cdot \nabla\eta$ P is the precipitation and E the evaporation (E). This is the so-called water flux boundary condition. b) The momentum boundary condition is:

$$A^v m \frac{\partial \boldsymbol{u}_h}{\partial z}\Big|_{z=\eta} = \frac{(\tau_u, \tau_v)}{\rho_0} \tag{14}$$

where $\tau_u, \tau_v$ are the zonal and meridional wind stress components respectively. c) The heat flux boundary condition is:

$$A^v T \frac{\partial T}{\partial z}\Big|_{z=0} = \frac{Q}{\rho_0 C_p} \tag{15}$$

where $C_p$ =4000 J/(kg° K) and $Q$ (W/m$^2$) is the non penetrative net heat flux at the surface. In our case, all the heat is assumed to be absorbed at the surface.

c) The boundary condition for the salinity is:

$$\rho A^{vS} \frac{\partial S}{\partial z}\Big|_{z=0} = (E - P) S \rho_0 \tag{16}$$



OSD
4, 213–244, 2007

where $S$ is the surface salinity which corresponds to the water flux condition (13).

The water flux has been chosen as:

$$\rho_0(E-P) = \gamma^{-1}\frac{(S-S*)}{S} \tag{17}$$

where $S$ is the model surface salinity, $S^*$ is the climatological surface salinity and $\gamma = -0.007$ $(m^2 s/kg)$ is the salinity relaxation coefficient. The corresponding relaxation time is:

$$\frac{1}{\rho_0}\gamma^{-1}\frac{(S-S*)}{S} = \frac{\Delta z}{\Delta t}$$

$$\Delta t = \rho_0 \Delta z \gamma \left(\frac{S}{S-S*}\right) \tag{18}$$

If $\Delta z = 3\ m$ is the first model layer depth, $\Delta t \cong 5$ days.

## 2.4 The Atlantic box and the Strait of Gibraltar

The model domain shown in Fig. 1 extends in the Atlantic and this part is called the Atlantic box. This box is necessary in order to properly simulate the exchange of water masses at the Gibraltar Strait. Unfortunately, no operational model has been available up to now where the lateral boundary conditions could be taken to drive the Atlantic box. Thus the latter now considers relaxation to climatology and vanishing currents at the last boundary point. The model salinity and temperature fields along a strip at the latitudinal and longitudinal boundaries of the Atlantic box (Fig. 1) are relaxed at all depths to the climatology with the terms introduced in the equations (3) and (6). The strip is an area with an extension of 2° at the westward and southward boundaries and 3° at the northern boundary (in order to cover all the area of the Gulf of Biscay).

The $\mu$ coefficient is spatially varying while $\delta$ is a time factor: $\mu$ is larger closer to the boundary points of the box and linearly decreases to zero outside the strip and $\delta = 2.3 \times 10^{-7}\ s^{-1}$. The horizontal diffusivities are also incremented by a factor of 5 in the Atlantic box strip areas in order to add a sponge layer.



OSD
4, 213–244, 2007

At the Strait of Gibraltar, between 6.25° W and 5.125° W the horizontal viscosity is laplacian instead of bilaplacian as in the rest of the model domain and the diffusivity is 10 times bigger than in the rest of the model domain. In the same geographical area the bottom friction drag coefficient is linear and ten times bigger then in the other parts of the model. Out of the Strait of Gibraltar in the Atlantic Box the bathymetry has been modified in order to resolve the Camarinam Sill (Sannino et al. 2004). These modification are necessary to avoid an unrealistic value of the transport at the Strait of Gibraltar.

### 2.5 The Water flux correction

The domain of Fig. 1 has closed boundaries and care should be taken in considering the effects of net sources/sinks of heat and water in the basin. In the Atlantic box, heat and salt is added or substracted by the relaxation terms in Eqs. (3) and (6) that are different from zero along the strip of the lateral boundaries, as described above. These terms will balance the heat loss and the salt gain from the sea surface, in particular over the Mediterranean part of the basin.

However care should be taken for the surface water boundary condition (13) which sets the sea surface height of the basin and thus the mass conservation. It is well known that the Mediterranean basin on a yearly average has a net water loss due to E exceeding P. The water lost at the surface of the Mediterranean Sea is balanced by a net inflow of water at the Gibraltar Strait. We need to enforce this balance so that the model volume does not drift.

The basin mean (E-P) is then separated into two components, the Atlantic and Mediterranean:

$$E - P = (E - P)_{\mathrm{MED}} + (E - P)_{\mathrm{ATL}} \tag{19}$$

At each time step the space integral of the Mediterranean and Atlantic water flux is



OSD
4, 213–244, 2007

computed and the sum of this two components of the water flux, $\Delta_{E-P}$, is computed:

$$\int_{x,y} (E-P)_{\mathrm{MED}} + \int_{x,y} (E-P)_{\mathrm{ATL}} = \Delta_{E-P} \quad (20)$$

will be used now to compute a new value of the water flux over the Atlantic in order to have the net water flux equal zero over the whole domain. This does not change the Mediterranean basin water loss but it balances it so that mass is conserved. A value of $(E-P)_{\mathrm{ATL\_CORR}}$ is therefore recomputed for each Atlantic grid point in the following way:

$$(E-P)_{\mathrm{ATL\_CORR}} = \Delta_{E-P}/AREA_{\mathrm{ATL}} - (E-P)_{\mathrm{ATL}} \quad (21)$$

where $AREA_{\mathrm{ATL}}$ is the Atlantic surface area. This assumption could be done only if the model in not used for climate simulations which cover hundreds of years, period over which the modification of the water flux into the Atlantic box could be relevant and non negligible. Figure 2 shows the value of $\Delta_{E-P}$ computed as percentage of the $(E-P)_{\mathrm{ATL\_CORR}}$ in one of the experiments studied in this paper. This value after the first months of simulation decreases and assumes a value of ca. 0.005%. This value is small enough and moreover doesn't increase during the simulation. Therefore we argue that this approximation, is valid for short term forecasting purposes. A new model is now being set where the lateral boundaries are nested in a coarser model of the global ocean and a modified correction is being implemented.

## 3 Design of the numerical experiments

The model described in Sect. 2 has been run with two different approximations of the atmospheric forcing:

1) the first, the so-called perpetual year forcing, where the water, heat and momentum surface fluxes are monthly varying climatological mean values;

2) the second with 6 h meteorological forcing for the period January 1997 to December 2004.



OSD
4, 213–244, 2007

In the following we describe the model design for each of these experiments.

### 3.1 Perpetual year experiment (P)

The perpetual year experiment, hereafter called P, considers seasonally repeating heat, water and momentum fluxes at the sea surface. The model has been initialized with a salinity and temperature field from the January monthly mean of MEDATLAS climatology (MEDAR/MEDATLAS Group, 2002) and with zero velocity field. A detailed description of the wind stress climatology, composed of monthly mean wind stresses previously computed, is given in the Appendix. This wind stress climatology is used in (14).

In the perpetual year simulation, Q in (15) is defined as:

$$Q = Q_0 + \frac{dQ}{dT}(T - T*) \tag{22}$$

where $Q_0$ is the net heat flux from the monthly mean climatology (described in the Appendix), T is the model surface temperature, $T^*$ is the climatological surface temperature (see Appendix) and is the relaxation coefficient. The heat flux relaxation time $\Delta\tau$corresponding to the relaxation factor is:

$$\frac{dQ/dT}{\rho_0 C_p} = \frac{\Delta z}{\Delta \tau} \quad \Delta\tau = \Delta z \frac{\rho_0 Cp}{dQ/dT} \tag{23}$$

Since the model surface layer thickness is $\Delta z = 3$ m then $\Delta\tau \cong 3,5$ days.

### 3.2 Interannual forcing experiment (I)

In the interactive physics experiments the wind stress for (14) is calculated interactively starting from 6 h surface meteorological fields from ECMWF using bulk formulas.

For the wind stress the surface winds are transformed in stress using the Hellerman & Rosenstein (1983) bulk parameterization and they are used in (14).



OSD
4, 213–244, 2007



EGU

For the heat flux in (15) we use:

$$Q = Q_S - Q_B(T_a, T_0, C, rh) - LE(T_a, T_0, rh, |\boldsymbol{v}_w|) \quad (24)$$

where the term on the right-hand site are: the net short wave incoming radiation, $Q_S$, the net long wave ri-emitted by the surface, $Q_B$, the latent, $LE$ and the sensible heat flux, $H$. They depend upon the air temperature at 2 m, $T_a$, the sea surface temperature computed by the model, $T_0$, the total cloudiness, $C$, the relative humidity computed from the dew point temperature at 2 m, $rh$, the 10m wind velocity amplitude, $|\boldsymbol{v}_w|$. The different heat bulk expressions for these terms were determined by Castellari et al. (2000) and verified later to give accurate long term heat budgets with ECMWF by Pinardi and Masetti (2000). Synthetically the bulk formulations used are: the Smitsonian astronomical formulas modified by Reed (1977) for $Q_S$, the Bignami et al. (1995) for $Q_B$, the Gill (1982) for $LE$ and Kondo (1975) for $H$ fluxes.

This experiment is hereafter called Interannual-I. The model initial condition for I is the December 31 mean daily value from the P experiment.

## 4 Model results and comparison with data

Both experiments have been studied and intercompared between themselves and with observations. One of the key indices of the circulation, is the value of the kinetic energy over the Mediterranean basin. The Atlantic box circulation is neglected because we consider the Atlantic box as a parameterization of large scale effects. The kinetic energy (KE) as been computed as:

$$KE = \frac{1}{V}\int_v \frac{1}{2}(u^2 + v^2)dV \quad (25)$$

where $u$ and $v$ are respectively the simulated zonal and meridional velocity field components and V is the volume of the basin. Figure 3 shows the values of KE for (P) and (I). The values increase during the first months of simulation in both experiments. The

KE reaches a more or less stable value in (P) after the third year of integration. The values for the experiment (I) seems to reach a statistically flat trend after the first two years of run. We need to note that the (I) experiment starts out of the sixth year of the (P) experiment. The values of KE are higher and with more variability in (I) than in (P) as it is expected due to the fact that (I) is forced by the atmospheric large scale interannual variability (P).

The first two years of (I) could be considered the time necessary for the model spin-up, therefore in the following sections show only the results from year 1999. The sixth year of perpetual simulation will be considered as the reference year for (P).

The model results have been compared first with independent data sets for the heat and wind stress forcing. Figure 04 shows a time series of the total heat flux, described in (24) and computed as basin mean for (P) and (I). The model values are compared with the NCEP/NCAR re-analysis values (Kalnay et al.,1996). (P) does has lower values than NCEP/NCAR during the summer but it reproduces rather faithfully the seasonal cycle. (I) at the contrary reproduces well the summer and it shows a large interannual variability in the winter fluxes as expected. Overall we can say that the model is forced by consistent heat fluxes both in the (P) and (I) experiments.

The monthly wind stress (WS) mean over the basin is now analysed together with the wind stress curl (WC) defined as:

$$WC = \frac{1}{A}\int_A \left(\frac{\partial \tau_v}{\partial x} - \frac{\partial \tau_u}{\partial y}\right) dA \tag{26}$$

and the wind stress has been defined in (14).

Figure 5 shows WS and WC computed for both the experiment (P) and (I). The values of WS of (P) have been compared with the WS computed from the NCEP/NCAR data. The major difference between (P) and NCEP/NCAR data is during summer. NCEP/NCAR shows a summer minimum while (P) reaches a secondary maximum during the same period. Examining the wind stress pattern (not shown) we note that the large amplitude meridional winds characterising the summer regimes over the Eastern



OSD
4, 213–244, 2007

Mediterranean are very weak in the NCEP/NCAR climatology and this could explain the difference. The (P) forcing, calculated from ECMWF re-analysis (Korres et al. 2000) have instead the large amplitude signal of the Etesian winds.

The panel in the middle represents the WS from (I) over the years 1999–2004 compared with (P). Both curves show a large seasonal signal but (I) shows a higher amplitude especially during winter. The first three years are characterized by lower values of WS with respect the last three years. The lower panel shows WC from (P) and (I). The values of WC are characterized by a seasonal signal and are for the Mediterranean basin mainly positive (as the basin is forced to have a cyclonic vorticity input). The year 2002, 2003 and 2004 have the largest WC values. In conclusion we might say that the atmospheric forcing variability in the (P) and (I) reproduces the well known patterns and it is consistent with an independent data set.

Figure 6 shows a map of the wind stress curl computed as mean over (I) from 1999 till 2004. From the map is evident that except in the western part of the Gulf of Lion the curl is positive over vast areas of the northern basin sector and positive, but with smaller area coverage, in the southern part of the Mediterranean. This is the well known pattern of the wind stress curl over the Mediterranean (Pinardi and Masetti, 2000, Demirov and Pinardi, 2002) that has been advocated in the past to be the main cause for the cyclonic character of the basin scale general circulation with large departures and anticyclonic circulation prevailing in the southern and south-eastern part of the basin.

The mass transport at main Straits of the Mediterranean Sea is another important index of the basin scale circulation, connected also to deep and intermediate water formation processes in the basin. The two main Straits are the strait of Gibraltar which connects the Mediterranean sea with the Atlantic ocean and the Sicily Strait, subdividing the Mediterranean Sea into the western and eastern parts.

The transport at the Gibraltar Strait is characterized by the inflow of the surface Atlantic water, corresponding to low salinity and the outflow of salty Mediterranean waters below 150 m approximately. The strait of Gibraltar is 13 km wide in its narrower part and it has a maximum depth of 350m. It is difficult for a model with an horizontal



OSD
4, 213–244, 2007



EGU

resolution of ca. 7 km to well simulate the exchange at this strait. As explained in Sect. 2 special parameterizations have developed for this area. With a free surface model, the net transport is different from zero and the inflow should be bigger than the outflow to balance the net water loss at the sea surface. The eastward and westward transport at the Strait of Gibraltar it is computed as:

$$T_r = \int_A \boldsymbol{u}_h \cdot \hat{n} dA \tag{27}$$

where $\boldsymbol{u}_h$ is the horizontal velocity, $\hat{n}$ is the unit vector normal to the vertical section A. The net transport is the difference between the eastward and the westward components. It is shown in Figure 7 and seasonal cycle is large and reaches maximum values in autumn. Some years, during march, the net transport could be negative but the average values over the year is always positive. It is clear that the net transport has a large seasonal cycle with interannual fluctuations superimposed. The eastward and westward transport at the Strait of Gibraltar have more or less the same fluctuation. It's not evident a seasonal cycle but the variability is largely related to the wind stress (Beranger et al. 2005). The wind stress and wind stress curl monthly mean have been computed over the area between 6° W and 1° W of longitude, corresponding to the Alboran Sea, for the years 1999–2004. The lower panel of Fig. 7 shows the value of the wind stress and the wind stress curl superimposed with the eastward transport. It is evident how much the variability of the transport is strongly correlated with the wind stress curl, more then with the wind stress intensity. When the curl is strongly negative (positive) the transport is high (low). When the curl is negative (positive) the vorticity is anticyclonic (cyclonic) and the wind direction should be mainly eastward (westward). January 2001 has a high transport and the curl is negative while in december 2001 the transport reaches a minimum in it's value and the curl is strongly positive. The time series of the lower panel of Fig. 7 shows clearly how this correlation is well respected during all the period of study.

Figure 8 shows the transports at the Sicily Strait where the westward and eastward values have larger values than at Gibraltar, confirming the results by Pinardi et al.,

(1997) with lower resolution models. The net transport has values and shape comparable to the net transport at Gibraltar. The westward and eastward components have a high variability with high values of thansport in winter and lower in summer. The comparison with observation during the years 1999–2001 (Beranger et al., 2004) agrees very well for the time variability and for the values reached during the period where the transport has high values. For example the maximum at the beginning of year 2001 evidenced from observation is well reproduced by the model simulation. The model seems to over estimates instead the minimum values of the transport wich are around 0.7 Sv during the period of 1999–2001 from the observation and never less then 1 Sv from the model simulation for the same period.

Another way to assess the interannual model performance is to compare the satellite Sea Level Anomaly (SLA) time series with the model output. The model computes values of Sea Surface Height (SSH) without considering the steric effect because it solves the incompressible continuity equation described in (4). Mass changes do not create a three dimensional divergence and thus the steric effect is a diagnostic quantity for our model. The steric component has then been computed from the density field of the model and then added to the SSH. The upper part of Fig. 9 shows the values of the steric component for both (P) and (I). The values are very similar for the two experiments and the seasonal cycle is clear with higher values during the summer. The values oscillate between –40 cm in winter and +40 cm in summer. The area average values of SSH from the model are also shown in Fig. 9 and in this case the difference between (P) and (I) is evident. The signal ranges between –25 cm and +20 cm in (I) and –5 cm and +10 cm for (P) showing that the sea level interannual signal is half of the steric seasonal signal in the Mediterranean Sea. In other words sea level variations induced by large scale circulation changes produced by wind, water and heat fluxes over the Mediterranean Sea have half the amplitude of the steric seasonal effects.

The SLA from the model has been defined has the sum of the steric component and the model SSH with the six years time mean subtracted. This time mean is equivalent to subtract the mean sea level or mean dynamic topography of the model. This is done



OSD
4, 213–244, 2007

because the satellite altimetry values have such value subtracted too. The lower panel of Fig. 9 represent the comparison between (I) and the satellite data. (I) reproduces well the seasonal variability and part of the interannual variability but it is missing the high values during the late summer-autumn period.

Before coming a discussion about this mismatch we would like to show the comparison of the model simulation with in situ temperature and salinity profiles.

XBT and ARGO vertical profiles have been collected over year 2003 and 2004 in the frame of MFSTEP. The rms between data and model have been computed at different depths: 30, 150 and 300 m. The upper panel of Fig. 10 shows the rms for temperature. The rms from XBT (left panel) has values with an high variability especially at the surface and it could be due to the scarcity in space of the data. The rms with the argo (right panel) shows instead values lower than 0.5°C except in the summer where the error is much bigger at the depth of 30 m. This could be due to the misplacement of the thermocline in the model simulation. This situation is present also in the lower panel that shows the rms for the salinity. (Dobricic et al., 2006, this volume). The rms at 30 m is generally about 0.08 psu in September of both 2003 and 2004 it could reach value of 1.6–1.8 psu. At 150 and 300 m the rms doesn't have this fluctuation. The rms at 150 m has values close to 0.08 psu which oscillation that could reach values of 1.2 psu or decrease down to 0.02 psu. At 300 m the rms is about of 0.04 psu.

We can now try to understand the differences in late summer–autumn in Fig. 9. This is due mainly to two factors:

1. the wrong water flux during summer which is lacking the high evaporative fluxes during late summer and autumn;

2. the upper mixed layer physics which does not correctly reproduce the deep, hot and salty mixed layer during the summer-autumn period.

This interpretation is supported by both Fig. 9 and Fig. 10 results which show that the model has large model errors in the upper thermocline.



OSD
4, 213–244, 2007

Figure 11 represents the velocity field at 30 m as averaged over years 1999–2004. The model is able to reproduce the main circulation patterns of the Mediterranean sea as described from literature (Millot et al. 2005, Pinardi et al. 2004, Robinson et al. 1992).

## 5 Conclusions

The experiments, described in this study, confirm that the high resolution free surface model implemented in the first phase of the MFSTEP project has a good capability in reproducing the ocean dynamic of the Mediterranean sea. This study shows that model results are in agreement with the data and observations even do some parameterizations of the model should be performed. This is the case of the water flux that should be more realistic and, as pointed out in Sect. 4 also the capability of the model to correctly reproduce the deep, hot and salty mixed layer during the summer-autumn period. The computation of a SLA and the possibility to compare it with the satellite data is an important improvement respect the previous lower resolution and rigid lid models implemented over the Mediterranean sea.

## Appendix A

### Bathymetry and coastline

The Digital Bathymetric Data Base-Variable Resolution has been used to make the MFS1671 coastlines and bathymetry. DBDB-1 at 1' resolution has been used for the Mediterranean basin while for the Atlantic DBDB-2 and DBDB-5 have been used. The bathymetry file has been manually corrected along the Croatian coast by a comparison with detailed nautical charts. The bathymetry has been interpolated on the model horizontal and vertical grid and manually checked for isolated grid point, islands and straits and passages.



OSD
4, 213–244, 2007

## A1 Vertical levels distribution

The distribution of the unevenly distributed vertical levels should satisfy the criteria of consistency and accuracy of the numerical scheme (Treguier et al., 1996). The vertical distribution of the levels is computed in OPA by a function which has a nearly uniform vertical level distribution at the ocean top and bottom with a smooth hyperbolic tangent transition in between. Several level distributions have been computed in order to find the one that better reproduce the vertical shape of temperature and salinity profiles for the region. Particular attention has been paid to the intermediate layer resolution where the water masses are characterised by only 0.5°C anomalies in the western Mediterranean.

## A2 Temperature and salinity monthly mean climatology

MEDATLAS monthly mean climatology (MEDAR/MEDATLAS Group, 2002) and WOA98 (Levitus, 1998) gridded climatologies have been used respectively for the Mediterranean Sea and the Atlantic ocean. The merging between the two climatologies has been done in a region on the western side of the Strait of Gibraltar.

## A3 Wind stress and heat fluxes perpetual year climatology

The wind stress monthly mean climatology has been done with two different data set, one for the Atlantic part and one for the Mediterranean. The monthly mean wind stress for the Mediterranean sea has been computed by Korres and Lascaratos (2003) using the ECMWF re-analysis fields for the period 1979–1993. The monthly mean climatology from Hellerman & Rosestein (1983) has been used for the Atlantic box. A weight function depending on distance in longitude has been used to merge the two monthly data sets, then the data have been interpolated with a splines on the numerical ocean model grid.

The perpetual year climatology for the heat flux covers only the Mediterranean and



OSD
4, 213–244, 2007

for the Atlantic only the relaxation to climatological temperature is used (see text) The heat fluxes have been computed by Korres and Lascaratos (2003) using the COADS cloud cover data set for the period from 1980 till 1988 and the Reynolds SST.

## References


Beranger, K., Mortier, L., Gasparini, G. P., Gervasio, L., Astraldi, M., and Crepon, M.: The dynamics of the Sicily Strait: a comprehensive study from observations and model, Deep Sea Research II, 51, 411–440, 2004.

Beranger, K., Mortier, L., and Crepon, M.: Seasonal variability of water transport through the Straits of Gibraltar, Sicily and Corsica, derived from a high-resolution model of the Mediterranean circulation, Prog. Ocean. 66, 341–364, 2005.

Castellari, S., Pinardi, N., and Leaman, K.: A model study of air-sea interactions in the Mediterranean Sea, J. Mar. Syst., 18, 89–114, 2000.

Demirov, E., Pinardi, N., Fratianni, C., Tonani, M., Giacomelli, L., and De Mey, P.: Assimilation scheme of the Mediterranean Forecasting System: operational implementation, Ann. Geophys., 21, 1, 189–194, 2003.

Demirov, E. and Pinardi, N.: The simulation of the Mediterranean Sea circulation from 1979 to 1993. Part I: The interannual variability, J. Mar. Syst., 33–34, 23–50, 2002.

Dobricic, S., Pinardi, N., Adani, M., Tonani, M., Fratianni, C., Bonazzi, A., and Fernandez, V.: Daily oceanographic analyses by the Mediterranean basin scale assimilation system, in review, Ocean Science, 2007.

Hellerman, S. and Rosestein, M.: Normal monthly wind stress over the world ocean with error estimates, J. Phys. Oceanogr., 13, 1093–1104, 1983.

Kalnay, E., Kanamitsu, M., Kistler, R., Collins, W., Deeven, D., Gandin, L., Iredell, M., Saha, S., White, G., Wollen, J., Zhu, Y., Chelliah, M., Ebisuzaki, W., Higgins, W., Janoviak, J., Mo, K. C., Ropelewsy, C., Wang, J., Leetma, R., Reynold, Jenne, R., and Joseph, D.: The NCEP/NCAR 40-Years Reanalysis Project, Bull. Amer. Meteor. Soc. 77, 437–471, 1996.

Korres, G., Pinardi, N., and Lascaratos, A.: The ocean response to low frequency interannual atmospheric variability in the Mediterranean Sea: Part I: Sensitivity experiments and energy analysis, J. Climate 13, 705–731, 2000.

Korres, G. and Lascaratos, A.: A one-way nested, eddy resolving model of the Aegean and




OSD

4, 213–244, 2007

Levantine basins: Implementation and climatological runs, Ann. Geophisicae 21, 1, 205–220, 2003.
Madec, G., Delecluse, P., Imbard, M., and Levy, C.: OPA8.1 Ocean general Circulation Model reference manual. Note du Pole de modelisazion, Institut Pierre-Simon Laplace (IPSL), France, 11, 1998.
MEDAR/MEDATLAS Group: MEDAR/MEDATLAS 1998–2001 Mediterranean and Black Sea database of temperature, salinity and bio-chemical parameters and climatological atlas (4CDroms), European Commission Marine Science and Technology Programme, and internet server www.ifremer.fr/sismer/program/medarIFREMER/TMSI/IDM/SISMER Ed., Centre de Brest), 2002.
Millot, C. and Tapier-Letage, I.: Circulation in the Mediterranean Sea. Handbook of Environmental Chemistry, vol.5, Part K: 29-66, D=I 10.1007/b 107143, Springer-Verlag Berlin Heidelberg, 2005.
Pinardi, N., Allen, I., Demirov, E., De Mey, P., Korres, G., Lascaratos, A., Le Traon, P. Y., Maillard, C., Manzella, G., and Tziavos, C.: The Mediterranean ocean Forecasting System : first phase of implementation (1998–2001), Ann. Geophys., 21, 1, 3–20, 2003.
Pinardi, N. and Masetti, E. : Variability of the large scale general circulation of the Mediterranean Sea from observations and modelling: a review, Palaeo 158, 153–174, 2000.
Pinardi, N., Korres, G., Lascaratos, A., Roussenov, V., and Stanev, E.: Numerical simulation of the interannual variability of the Mediterranean Sea upper ocean circulation, Geophys. Res. Lett. 24, 425–428, 1997.
Pinardi N., Arneri, E., Crise, A., Ravaioli, M., and Zavatarelli, M.: The physical and ecological structure and variability of shelf areas in the Mediterranean Sea, “The Sea”, Vol. 14, Chapter 32, 2006.
Reed, R. K.: On estimating insolation over ocean, J. Phys. Oceanogr., 17, 854–871, 1977.
Robinson, A., Malanotte-Rizzoli, P., Hecht, A., Nichelato, A., Roether, W., Theocharis, A., Unluata, U., Pinardi, N., and the POEM Group: General circulation of the eastern Mediterranean, Earth Sciences Reviews, 285–309, 1992.
Roullet, G. and Madec, G. : Salt conservation, free surface, and varying levels: a new formulation for ocean general circulation models, J. G. R., 105, C10, 23 927–23 942, 2000.
Sannino, G., Bargagli, A., and Artale, V.: Numerical modeling of the semidiurnal tide exchange through the Starti of Gibraltar, J. Geophys. Res., 109, C=5011, 2004.
Treguier, A. M., Dukowicz, J. K., and Bryan, K.: Properties of nonuniform grid used in general

circulation models. J. Geophys. Res., 101, C9, 20 877–20 881, 1996.

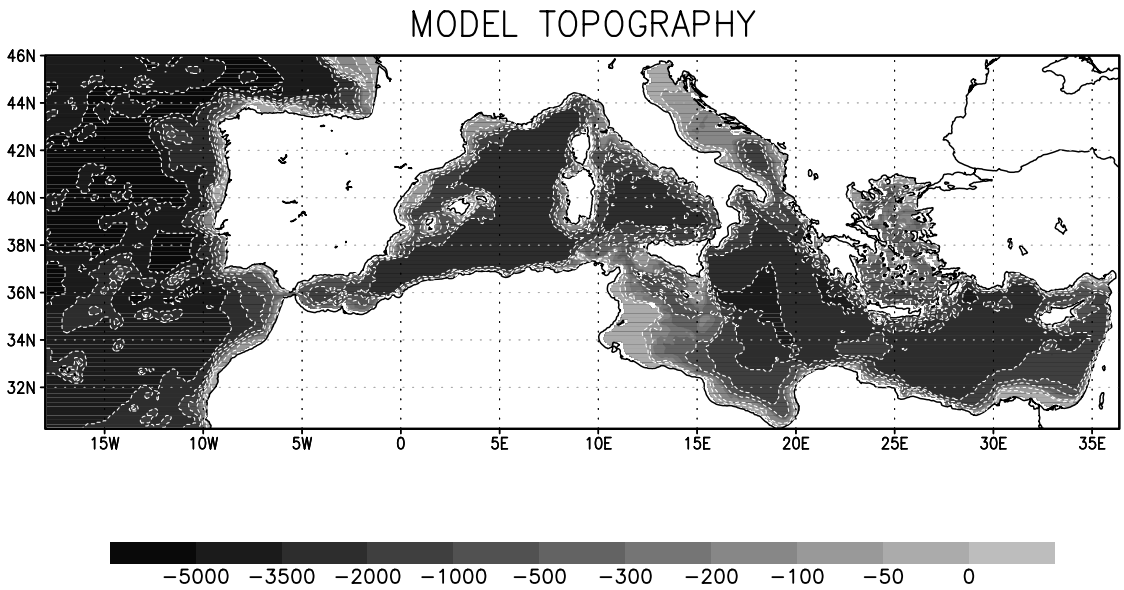


**Fig. 1.** Model bathymetry and domain.



OSD
4, 213–244, 2007



EGU

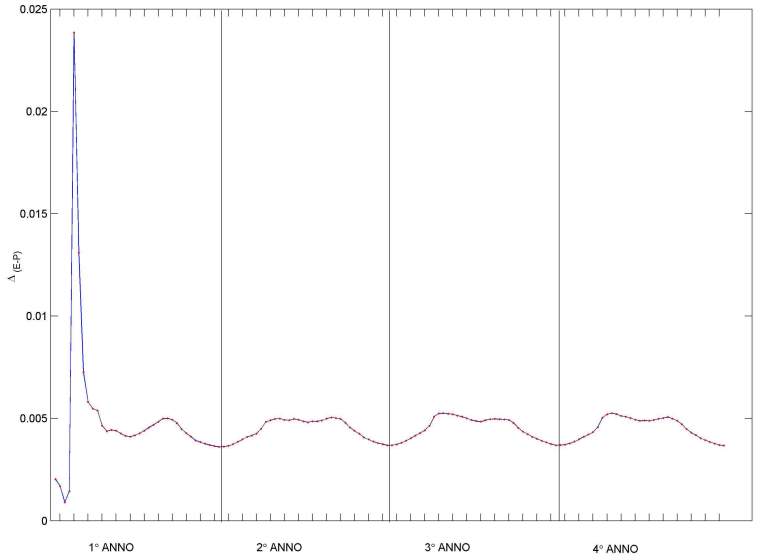


**Fig. 2.** Value of the water flux correction factor as a percentage respect the totals water flux in the atlantic box.



OSD
4, 213–244, 2007

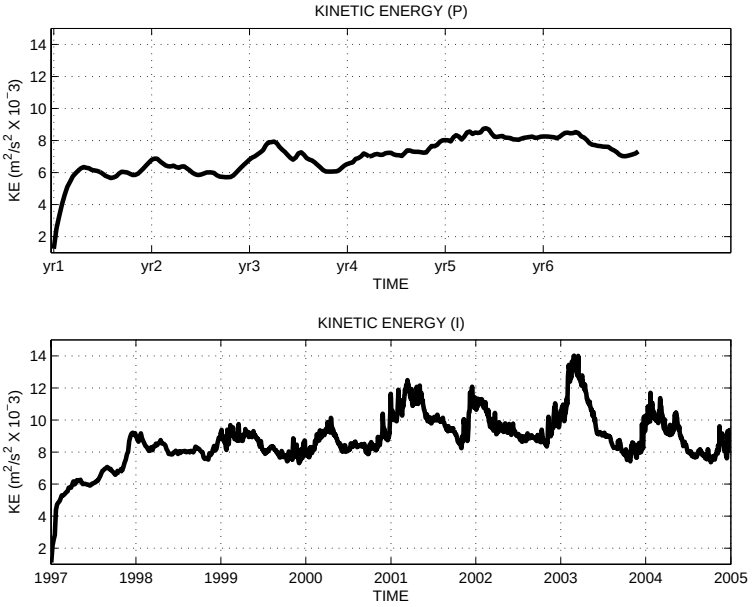


**Fig. 3.** Volume integral of the kinetic energy computed for the experiment (P) and (I).



OSD
4, 213–244, 2007

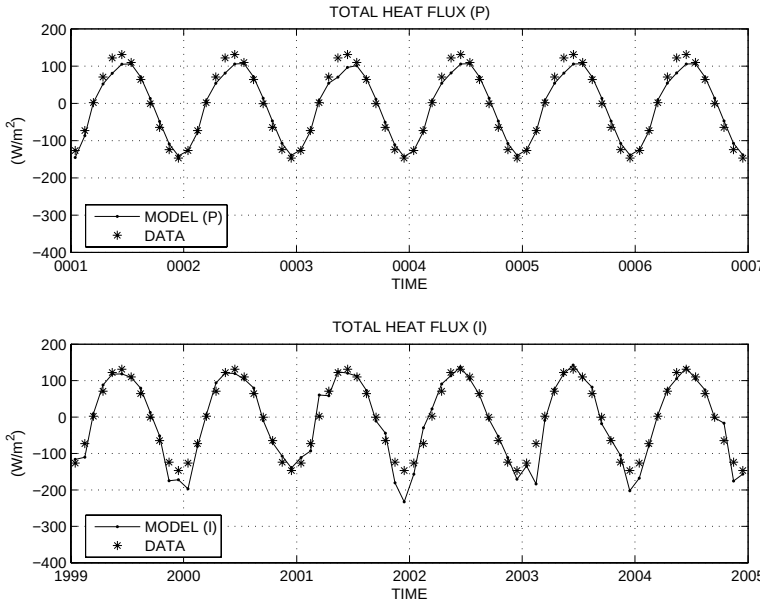


**Fig. 4.** Comparison between the total heat flux computed from the model experiments (P e I) and the NCEP NCAR reanalysis.



OSD
4, 213–244, 2007



EGU

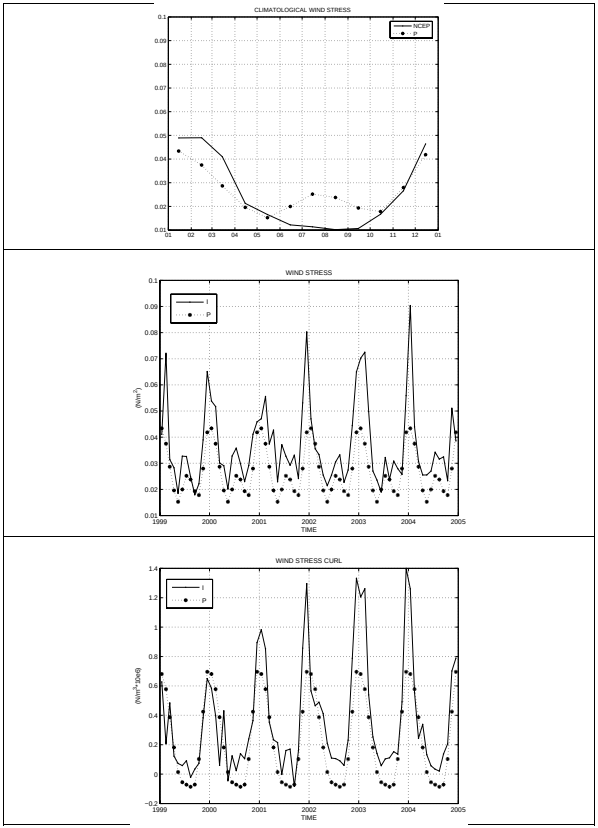


**Fig. 5.** Monthly mean basin averaged wind stress and wind stress curl computed from the model experiments (P) and (I) and from the NCEP/NCAR climatology.

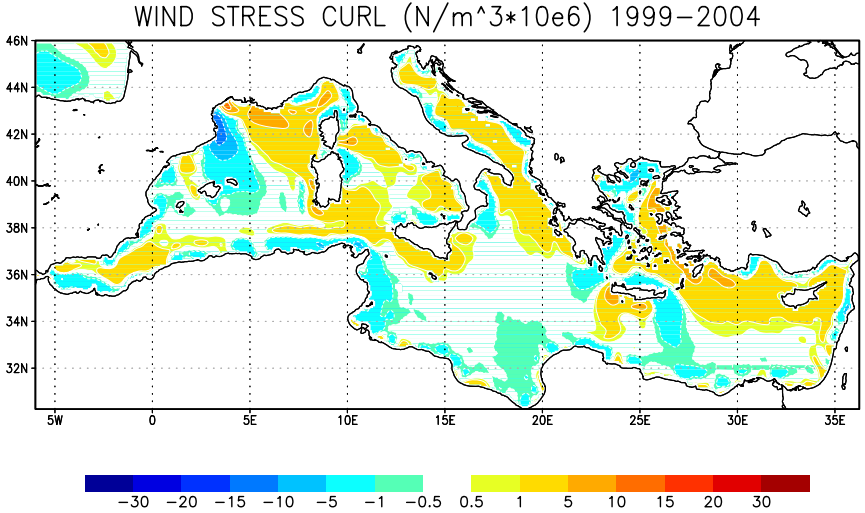


**Fig. 6.** Map of wind stress curl computed as average from the model experiments over the years 1999–2004.



OSD
4, 213–244, 2007



EGU

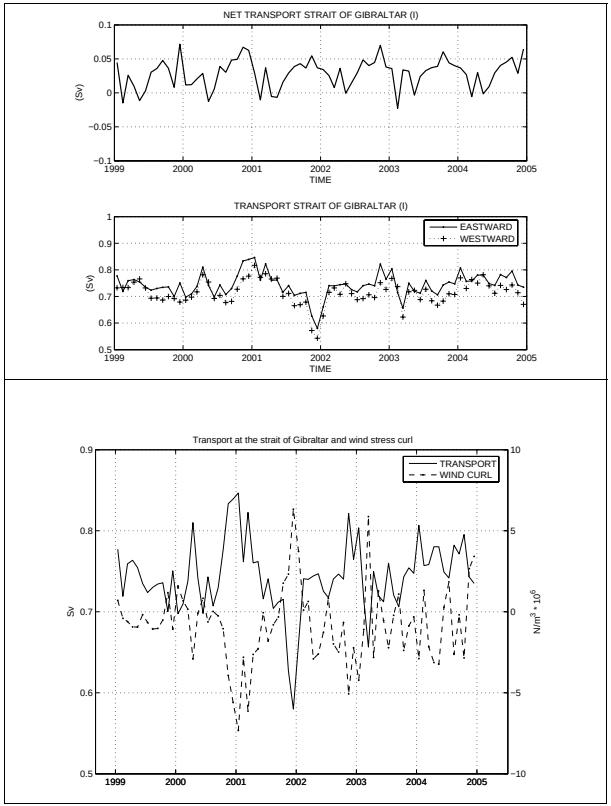


**Fig. 7.** Mass transport at the Strait of Gibraltar(net, eastward and westward) and wind stress and wind stress curl from experiment (I).



OSD
4, 213–244, 2007

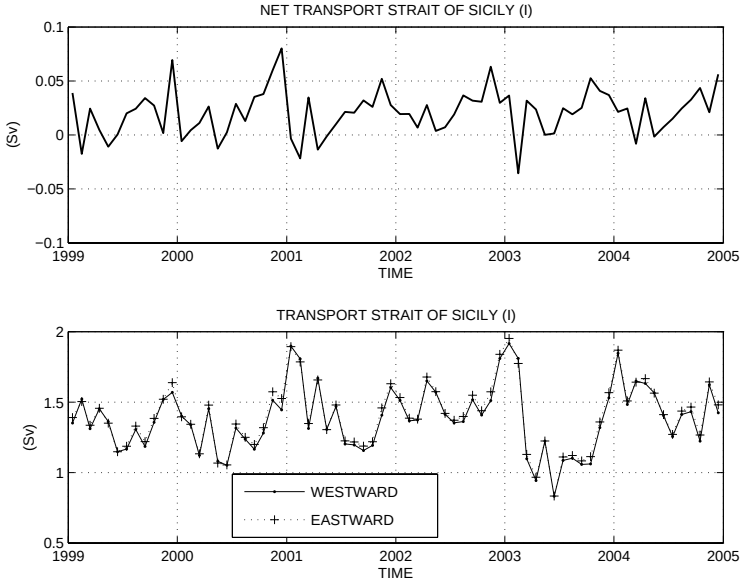


**Fig. 8.** Mass transport at the Strait of Sicily (net, eastward and westward) from experiment (I).



OSD
4, 213–244, 2007

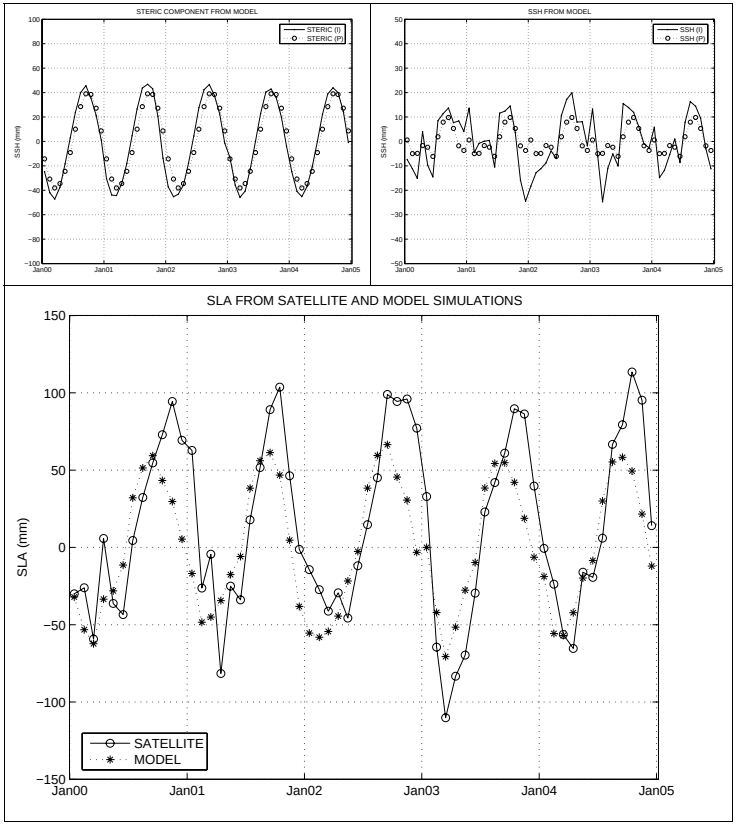


**Fig. 9.** Integral of ssh and steric component from the model experiments (P) and (I) and their comparison with the satellite data collected from year 2000 till 2004.



OSD
4, 213–244, 2007



EGU

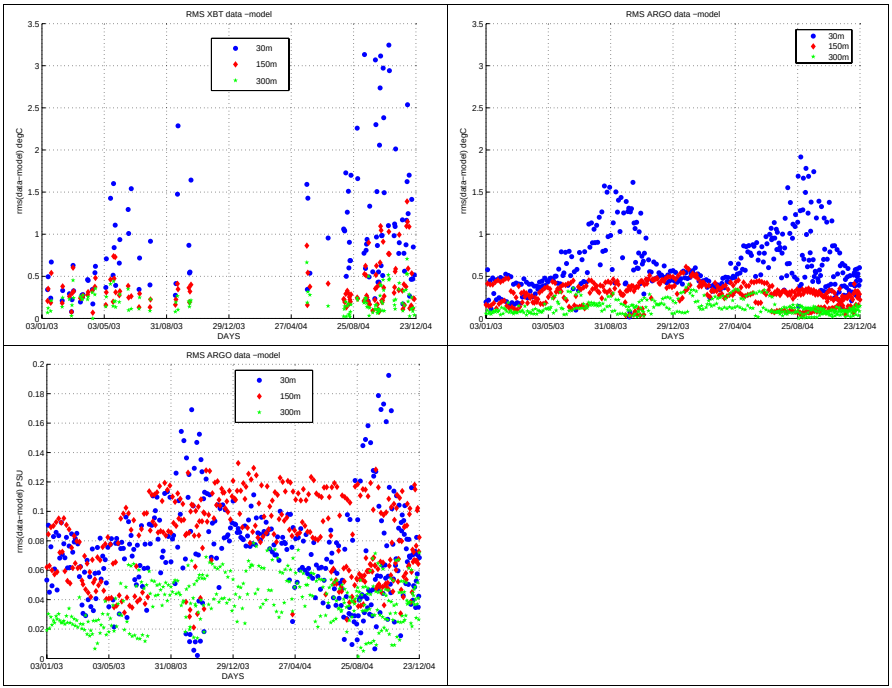


**Fig. 10.** Rms between data and model for year 2003 and 2004. The upper panel shows the rms of temperature at 30, 150 and 300 m depth computed from model and XBT and ARGO data. The lower panel shows the rms of salinity between the model and the ARGO.



OSD
4, 213–244, 2007



EGU

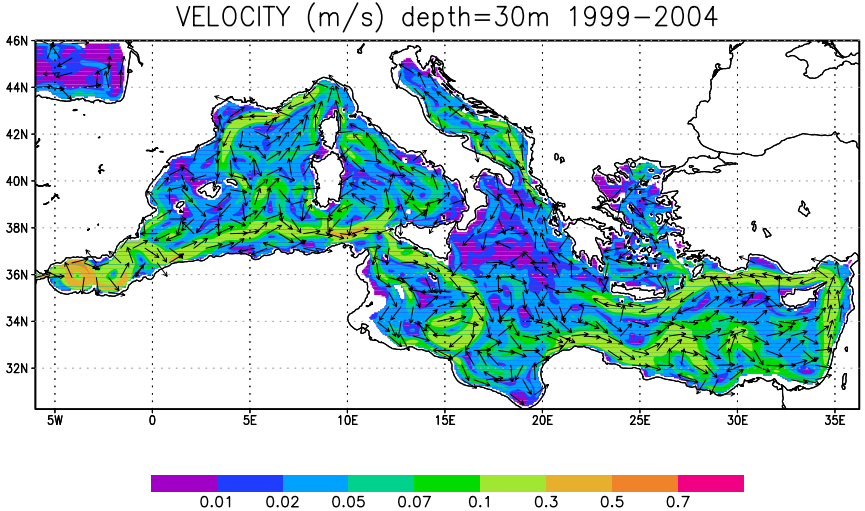


**Fig. 11.** Map of the circulation over the Mediterranean basin at 30 m computed as mean over the model simulation from year 1999 till 2004.



OSD
4, 213–244, 2007



EGU